Complexes with $Fe^{III}_2(\mu\text{-O})(\mu\text{-OH})$, $Fe^{III}_2(\mu\text{-O})_2$, and $[Fe^{III}_3(\mu_2\text{-O})_3]$ Cores: Structures, Spectroscopy, and Core Interconversions

Hui Zheng, Yan Zang, Yanhong Dong, Victor G. Young, Jr., and Lawrence Que, Jr.*

Contribution from the Department of Chemistry and Center for Metals in Biocatalysis, University of Minnesota, Minneapolis, Minnesota 55455

Received October 14, 1998

Abstract: We have synthesized the first complexes with bis(μ-oxo)diiron(III) and (μ-oxo)(μ-hydroxo)diiron(III) cores (**1** and **2**, L = TPA (**a**), 5-Et$_3$-TPA (**b**), 6-Me$_3$-TPA (**c**), 4,6-Me$_6$-TPA (**d**), BQPA (**e**), BPEEN (**f**), and BPMEN (**g**)) and found them to have novel structural properties. In particular, the presence of two single-atom bridges in these complexes constrains the Fe−Fe distances to 2.7−3.0 Å and the Fe−μ-O−Fe angles to 100° or smaller. The significantly acute Fe−O−Fe angles (e.g., 92.5(2)° for **1c** and 100.2(2)° for **2f**) enforced by the Fe_2O_2(H) core endow these complexes with UV−vis, Raman, and magnetic properties quite distinct from those of other (μ-oxo)diiron(III) complexes. Complex **1c** exhibits visible absorption bands at 470 (ϵ = 560 M^{-1} cm^{-1}) and 760 nm (ϵ = 80 M^{-1} cm^{-1}), while complexes **2** show features at ca. 550 ($\epsilon \approx$ 800 M^{-1} cm^{-1}) and ca. 800 nm ($\epsilon \approx$ 70 M^{-1} cm^{-1}), all of which are red shifted compared to those of other (μ-oxo)diiron(III) complexes. These complexes also exhibit distinct $\nu_{Fe-O-Fe}$ vibrations at ca. 600 and ca. 670 cm^{-1} assigned to the ν_{sym} and the ν_{asym} of the Fe−O−Fe units, respectively. The relative intensities of the ν_{sym} and ν_{asym} bands are affected by the symmetry of the Fe−O−Fe units; an unsymmetric core enhances the intensity of the ν_{asym}. Complexes **2** exhibit another band at ca. 500 cm^{-1}, which is assigned to the Fe−(OH)−Fe stretching mode due to its sensitivity to both $H_2{}^{18}O$ and ^2H_2O. Magnetic susceptibility studies reveal J = 54 cm^{-1} for **1c** and ca. 110 cm^{-1} for **2** ($\mathbf{H} = J\mathbf{S}_1\cdot\mathbf{S}_2$), values smaller than those for the antiferromagnetic interactions found in (μ-oxo)diiron(III) complexes. This weakening arises from the longer Fe−μ-O bonds and the smaller Fe−μ-O−Fe angles in the Fe_2O_2(H) diamond core structure. These spectroscopic signatures can thus serve as useful tools to ascertain the presence of such core structures in metalloenzyme active sites. These two core structures, $Fe_2(\mu\text{-O})_2$ (**1**) and $Fe_2(\mu\text{-O})(\mu\text{-OH})$ (**2**), can also be interconverted by protonation equilibria with pK_a's of 16−18 in CH_3CN. Furthermore, the $Fe_2(\mu\text{-O})_2$ core (**1**) isomerizes to the $Fe_3(\mu_2\text{-O})_3$ core (**7**), while the $Fe_2(\mu\text{-O})(\mu\text{-OH})$ core (**2**) exhibits aquation equilibria to the $Fe_2(\mu\text{-O})(\mu\text{-H}_3O_2)$ core (**5**), except for L = 6-Me$_3$-TPA and 4,6-Me$_6$-TPA. It is clear from these studies that electronic and steric properties of the ligands significantly affect the various equilibria, demonstrating a rich chemistry involving water-derived ligands alone.

Introduction

Nonheme diiron centers bridged by oxo (or hydroxo) and carboxylato groups have been found in methane monooxygenase (MMO),[1] ribonucleotide reductase (RNR),[2] and fatty acid desaturases.[3] These enzymes have elicited considerable interest due to their widespread occurrence and are involved in diverse functions such as the hydroxylation of methane, the generation of the catalytically essential Tyr radical for ribonucleotide reduction, and the desaturation of saturated fatty acids.[4] High-valent intermediates have been identified in the redox cycles of these oxygen-activating nonheme diiron enzymes; specifically, a diiron(IV) species named **Q** has been observed for MMO,[5] and an iron(III)iron(IV) species called **X** has been characterized for RNR.[6]

The $M_2(\mu\text{-O})_2$ diamond core is emerging as an important structural motif for stabilizing high oxidation states in nonheme enzymes.[7,8] Due to the presence of two oxo bridges, this motif is characterized by short M−O bonds (ca. 1.8 Å) and M−M distances of less than 3 Å that can be readily identified by EXAFS analysis.[7,9] On this basis, such high-valent cores have been found in the photosynthetic oxygen-evolving complex

(1) (a) Rosenzweig, A. C.; Frederick, C. A.; Lippard, S. J.; Nordlund, P. *Nature (London)* **1993**, *366*, 537−543. (b) Rosenzweig, A. C.; Nordlund, P.; Takahara, P. M.; Frederick, C. A.; Lippard, S. J. *Chem. Biol.* **1995**, *2*, 409−418. (c) Elango, N.; Radhakrishnam, R.; Froland, W. A.; Wallar, B. J.; Earhart, C. A.; Lipscomb, J. D.; Ohlendorf, D. H. *Protein Sci.* **1997**, *6*, 556−568.

(2) (a) Nordlund, P.; Eklund, H. *J. Mol. Biol.* **1993**, *232*, 123−164. (b) Logan, D. T.; Su, X.-D.; Åberg, A.; Regnström, K.; Hajdu, J.; Eklund, H.; Nordlund, P. *Struct. Bonding (Berlin)* **1996**, *4*, 1053−1064.

(3) Lindqvist, Y.; Huang, W.; Schneider, G.; Shanklin, J. *EMBO J.* **1995**, *15*, 4081−4092.

(4) (a) Feig, A. L.; Lippard, S. J. *Chem. Rev.* **1994**, *94*, 759−805. (b) Wallar, B. J.; Lipscomb, J. D. *Chem. Rev.* **1996**, *96*, 2625−2658.

(5) (a) Lee, S.-K.; Nesheim, J. C.; Lipscomb, J. D. *J. Biol. Chem.* **1993**, *268*, 21569−21577. (b) Lee, S.-K.; Fox, B. G.; Froland, W. A.; Lipscomb, J. D.; Münck, E. *J. Am. Chem. Soc.* **1993**, *115*, 6450−6451. (c) Liu, K. E.; Wang, D.; Huynh, B. H.; Edmondson, D. E.; Salifoglou, A.; Lippard, S. J. *J. Am. Chem. Soc.* **1994**, *116*, 7465−7466. (d) Liu, K. E.; Valentine, A. M.; Wang, D.; Huynh, B. H.; Edmondson, D. E.; Salifoglou, A.; Lippard, S. J. *J. Am. Chem. Soc.* **1995**, *117*, 10174−10185.

(6) (a) Bollinger, J. M.; Edmondson, D. E.; Huynh, B. H.; Filley, J.; Norton, J.; Stubbe, J. *Science (Washington, D. C.)* **1991**, *253*, 292−298. (b) Ravi, N.; Bollinger, J. M.; Huynh, B. H.; Edmondson, D. E.; Stubbe, J. *J. Am. Chem. Soc.* **1994**, *116*, 8007−8014. (c) Sturgeon, B. E.; Burdi, D.; Chen, S.; Huynh, B. H.; Edmondson, D. E.; Stubbe, J.; Hoffman, B. M. *J. Am. Chem. Soc.* **1996**, *118*, 7551−7557.

(7) Yachandra, V. K.; Sauer, K.; Klein, M. P. *Chem. Rev.* **1996**, *96*, 2927−2950.

(8) Que, L., Jr. *J. Chem. Soc., Dalton Trans.* **1997**, 3933−3940.

(9) Que, L., Jr.; Dong, Y.; Shu, L.; Wilkinson, E. C. In *Spectroscopic Methods in Bioinorganic Chemistry*; Solomon, E. I., Hodgson, K. O., Eds.; Oxford University Press: New York, 1998; Vol. 692, p 374.

10.1021/ja983615t CCC: $18.00
Published on Web 03/02/1999

(OEC) and are proposed to be components of the tetramanganese cluster responsible for the oxidation of water to O_2.[7,10] A related core has also been recognized in the inactive superoxidized form of Mn-catalase.[11] An $Fe_2(\mu\text{-}O)_2$ core structure is also one of the structures proposed to account for the 2.5-Å Fe−Fe distances found for intermediates **Q** and **X** of MMO and RNR, respectively.[12,13]

There are numerous synthetic precedents for the $M_2(\mu\text{-}O)_2$ diamond core in the literature, particularly for M = Mn. $Mn_2(\mu\text{-}O)_2$ cores are well characterized with $Mn^{III}Mn^{III}$, $Mn^{III}Mn^{IV}$, and $Mn^{IV}Mn^{IV}$ oxidation states.[14] This array of complexes has provided the structural foundation for interpreting the spectroscopic properties observed for Mn-catalase[11] and the Mn cluster of the OEC.[7,10,15] It is clear that the oxo bridges play an important role in stabilizing the higher valent states. The first examples of high-valent copper and iron complexes with $M_2(\mu\text{-}O)_2$ cores have only been synthesized in the past few years. $[Cu^{III}_2(\mu\text{-}O)_2]^{2+}$ complexes have been obtained from the reaction of O_2 and copper(I) complexes of bidentate and tridentate amine ligands.[16] In the course of the reaction, O_2 undergoes a four-electron reduction, and two Cu^I centers are oxidized to the Cu^{III} state. $[Fe^{III}Fe^{IV}(\mu\text{-}O)_2]^{3+}$ complexes have been obtained by us from the reaction of H_2O_2 with (μ-oxo)diiron(III) complexes of the tetradentate tripodal ligand TPA or its ring-alkylated derivatives.[17−19] However, these metastable complexes can only be prepared and characterized at low temperatures, and only very recently has one example been crystallized.[20]

The first crystallographically characterized complex with an $Fe_2(\mu\text{-}O)_2$ diamond core is the diiron(III) complex, $[Fe_2(\mu\text{-}O)_2(6\text{-}Me_3\text{-}TPA)_2](ClO_4)_2$ (**1c**),[21,22] which derives from the deprotonation of its conjugate acid, $[Fe_2(\mu\text{-}O)(\mu\text{-}OH)(6\text{-}Me_3\text{-}TPA)_2](ClO_4)_3$ (**2c**), a complex with the novel $Fe_2(\mu\text{-}O)(\mu\text{-}OH)$ core.[23] These complexes fit into an even larger array of (μ-oxo)diiron(III) complexes with water ligands in different dissociation states, that are related by acid−base chemistry and aquation equilibria (Scheme 1). The relative stabilities of these complexes vary with the ligands, allowing us to characterize structurally a number of these cores by suitable choice of ligand. Indeed, some of these core structures can be found in the active sites of the nonheme diiron enzymes in the diiron(III) oxidation state. This paper reports details of the syntheses and structures of $[Fe_2(\mu\text{-}O)_2(6\text{-}Me_3\text{-}TPA)_2](ClO_4)_2$ (**1c**), the related $[Fe_3(\mu_2\text{-}O)_3(5\text{-}Et_3\text{-}TPA)_3](ClO_4)(BPh_4)_2$ (**7b**), and corresponding conjugate acid complexes with an $Fe^{III}_2(\mu\text{-}O)(\mu\text{-}OH)$ diamond core. A systematic study of the acid−base chemistry of the (μ-oxo)diiron(III) complexes is also presented. Most importantly, the acute Fe−O−Fe angles enforced by the $Fe_2O_2(H)$ cores give rise to novel spectroscopic and magnetic properties that serve as useful signatures for such core structures.

Scheme 1

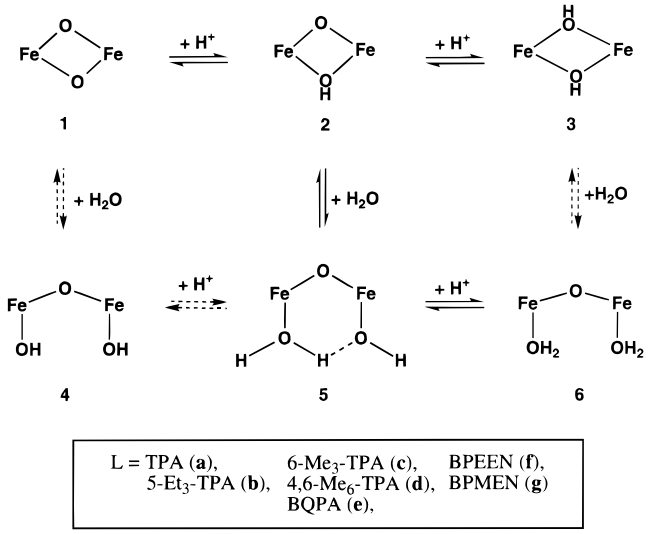

Experimental Section

Syntheses. The ligands TPA,[17] 5-Et_3-TPA,[17] 6-Me_3-TPA,[24] BQPA,[25] BPEEN,[26] and BPMEN[26] were synthesized according to literature methods. Commercially available chemicals were purchased and used without further purification. Elemental analyses were performed at M-H-W Laboratories (Phoenix, AZ). ***Caution***: Perchlorate salts are potentially explosive and should be handled with care!

2-(Chloromethyl)-4,6-dimethylpyridine hydrochloride (i) and 2-(aminomethyl)-4,6-dimethylpyridine hydrochloride (ii) were prepared using 2,4,6-collidine as starting material following procedures described in ref 27. ^{1}H NMR (D_2O): **(i)** δ (ppm) 7.55 (s, 1H), 7.46 (s, 1H), 4.68 (s, 2H), 2.54 (s, 3H), 2.41 (s, 3H); **(ii)** δ (ppm) 7.51 (s, 2H), 4.64 (s, 2H), 2.54 (s, 3H), 2.42 (s, 3H).

Tris(4,6-dimethyl-2-pyridylmethyl)amine. A mixture of 1.49 g (7.74 mmol) of **i** and 0.81 g (3.87 mmol) of **ii** in water (10 mL) was

(10) Yachandra, V. K.; DeRose, V. J.; Latimer, M. J.; Mukerji, I.; Sauer, K.; Klein, M. P. *Science* **1993**, *260*, 675−679.

(11) (a) Waldo, G. S.; Yu, S.; Penner-Hahn, J. E. *J. Am. Chem. Soc.* **1992**, *114*, 5869−5870. (b) Dismukes, G. C. In *Bioinorganic Catalysis*; Reedjik, J., Ed.; Marcel Dekker: Amsterdam, 1992; pp 317−346. (c) Gamelin, D. R.; Kirk, M. L.; Stemmler, T. L.; Pal, S.; Armstrong, W. H.; Penner-Hahn, J. E.; Solomon, E. I. *J. Am. Chem. Soc.* **1994**, *116*, 2392−2399.

(12) Shu, L.; Nesheim, J. C.; Kauffmann, K.; Münck, E.; Lipscomb, J. D.; Que, L., Jr. *Science* **1997**, *275*, 515−518.

(13) Riggs-Gelasco, P. J.; Shu, L.; Chen, S.; Burdi, D.; Huynh, B. H.; Que, L., Jr.; Stubbe, J. *J. Am. Chem. Soc.* **1998**, *120*, 849−860.

(14) Manchanda, R.; Brudvig, G. W.; Crabtree, R. H. *Coord. Chem. Rev.* **1995**, *144*, 1−38.

(15) Kirby, J. A.; Roberson, A. S.; Smith, J. P.; Thompson, A. C.; Cooper, S. R.; Klein, M. P. *J. Am. Chem. Soc.* **1981**, *103*, 5529−5537.

(16) (a) Mahapatra, S.; Halfen, J. A.; Wilkinson, E. C.; Pan, G.; Cramer, C. J.; Que, L., Jr.; Tolman, W. B. *J. Am. Chem. Soc.* **1995**, *117*, 8865−8866. (b) Halfen, J. A.; Mahapatra, S.; Wilkinson, E. C.; Kaderli, S.; Young, V. G., Jr.; Que, L., Jr.; Zuberbühler, A. D.; Tolman, W. B. *Science* **1996**, *271*, 1397−1400. (c) Mahapatra, S.; Young, V. G., Jr.; Kaderli, S.; Zuberbühler, A. D.; Tolman, W. B. *Angew. Chem., Int. Ed. Engl.* **1997**, *36*, 130−133. (d) Mahadevan, V.; Hou, Z.; Cole, A. P.; Root, D. E.; Lal, T. K.; Solomon, E. I.; Stack, D. P. *J. Am. Chem. Soc.* **1997**, *119*, 11996−11997. (e) Mahapatra, S.; Halfen, J. A.; Wilkinson, E. C.; Pan, G.; Wang, X.; Young, V. G., Jr.; Cramer, C. J.; Que, L., Jr.; Tolman, W. B. *J. Am. Chem. Soc.* **1996**, *118*, 11555−11574.

(17) Dong, Y.; Fujii, H.; Hendrich, M. P.; Leising, R. A.; Pan, G.; Randall, C. R.; Wilkinson, E. C.; Zang, Y.; Que, L., Jr.; Fox, B. G.; Kauffmann, K.; Münck, E. *J. Am. Chem. Soc.* **1995**, *117*, 2778−2792.

(18) Dong, Y.; Que, L., Jr.; Kauffmann, K.; Münck, E. *J. Am. Chem. Soc.* **1995**, *117*, 11377−11378.

(19) Dong, Y.; Zang, Y.; Shu, L.; Wilkinson, E. C.; Kauffman, K.; Münck, E.; Que, L., Jr. *J. Am. Chem. Soc.* **1997**, *119*, 12683−12684.

(20) Hsu, H.-F.; Shu, L.; Dong, Y.; Young, V. G., Jr.; Que, L., Jr. Submitted.

(21) Abbreviations used: BQPA, bis(2-quinolylmethyl)(2-pyridylmethyl)amine; BPEEN, *N*,*N*′-diethyl-*N*,*N*′-bis(2-pyridylmethyl)ethane-1,2-diamine; BPMEN, *N*,*N*′-dimethyl-*N*,*N*′-bis(2-pyridylmethyl)ethane-1,2-diamine; N5, *N*-(hydroxyethyl)-*N*,*N*′,*N*′-tris(2-benzimidazolylmethyl)-1,2-diaminoethane; 2,4-lut, 2,4-lutidine; Phen, phenanthroline; Me_3TACN, 1,4,7-trimethyl-1,4,7-triazacyclononane; 4,6-Me_6-TPA, tris(4,6-dimethyl-2-pyridylmethyl)amine; 5-Et_3-TPA, tris(5-ethyl-2-pyridylmethyl)amine; 6-Me_3-TPA, tris(6-methyl-2-pyridylmethyl)amine; TPA, tris(2-pyridylmethyl)amine.

(22) Zang, Y.; Dong, Y.; Que, L., Jr.; Kauffmann, K.; Münck, E. *J. Am. Chem. Soc.* **1995**, *117*, 1169−1170.

(23) Zang, Y.; Pan, G.; Que, L., Jr.; Fox, B. G.; Münck, E. *J. Am. Chem. Soc.* **1994**, *116*, 3653−3654.

(24) Zang, Y.; Kim, J.; Dong, Y.; Wilkinson, E. C.; Appleman, E. H.; Que, L., Jr. *J. Am. Chem. Soc.* **1997**, *119*, 4197−4205.

(25) Wei, N.; Murthy, N. N.; Chen, Q.; Zubieta, J.; Karlin, K. D. *Inorg. Chem.* **1994**, *33*, 1953−1965.

(26) Toftlund, H.; Pedersen, E.; Yde-Andersen, S. *Acta Chem. Scand., Ser. A* **1984**, *38*, 693−694.

(27) Nanthakumar, A.; Fox, S.; Murthy, N. N.; Karlin, K. D. *J. Am. Chem. Soc.* **1997**, *119*, 3898−3906.

Table 1. Crystallographic Experiments and Computations for **1c**, **2c**, **2e**, **2f,** and **7b**

	1c·2THF	**2c**·THF	**2e**·CH_3CN	**2f**·CH_3CN·1.5THF	**7b**·$2CH_3CN$
formula	$C_{50}H_{64}Cl_2Fe_2N_8O_{12}$	$C_{46}H_{57}Cl_3Fe_2N_8O_{15}$	$C_{54}H_{48}Cl_3Fe_2N_9O_{14}$	$C_{44}H_{68}Cl_3Fe2N_9O_{15.5}$	$C_{124}H_{130}B_2ClFe_3N_{14}O_7$
formula weight, amu	1151.69	1179.04	1264.04	1189.12	2153.09
crystal habit, color	wedge, dark red	prism, black	block, brown-red	block, brown-red	block, brown
crystal system	monoclinic	monoclinic	monoclinic	orthorhombic	monoclinic
space group	$P2_1/n$	$P2_1/c$	$P2/n$	$Fdd2$	Cc
a, Å	13.222(3)	21.550(4)	13.5119(6)	26.1539(1)	25.5756(1)
b, Å	14.062(3)	18.984(4)	11.3219(5)	64.6139(3)	14.4026(2)
c, Å	14.818(3)	12.421(3)	18.6779(8)	12.7408(1)	31.4563(1)
β, deg	112.76(3)	93.55(3)	103.7856(1)	90	105.625(1)
V, Å^3	2540.5(9)	5072(2)	2775.1(2)	21530.7(2)	11158.9(2)
Z	2	4	2	16	4
D(calcd), g cm^{-3}	1.506	1.544	1.513	1.467	1.285
temperature, K	173	173	173	173	173
λ, Å	0.710 73	0.710 73	0.710 73	0.710 73	0.710 73
R^a	0.0656	0.0685	0.067	0.0485	0.0656
$R_w{}^b$	0.1468	0.1568	0.1410	0.1327	0.1156

[a] $R = (\sum||F_o| - |F_c||)/(\sum|F_o|)$. [b] $R_w = (\sum[w(F_o^2 - F_c^2)^2]/\sum[wF_o^4])^{1/2}$, where $w = q/\sigma^2(F_o^2) + (aP)^2 + bP$.

neutralized by dropwise addition of NaOH (0.93 g, 23.22 mmol) in water (10 mL) at 0 °C. This solution was stirred at room temperature for 3 days, during which time an oil formed in the solution. The oil was extracted into CH_2Cl_2 (30 mL) and dried over Na_2SO_4. The CH_2Cl_2 extract was stripped to dryness by rotary evaporation to yield an off-white solid. The pure product (1.15 g, 80% yield) was obtained following column chromatography on alumina (eluant, CH_2Cl_2). ^{1}H NMR ($CDCl_3$): δ (ppm) 6.78 (s, 6H), 3.85 (s, 6H), 2.50 (s, 9H), 2.36 (s, 9H).

[Fe_2(O)(OH)(6-Me_3-TPA)$_2$](ClO_4)$_3$ (2c). To a solution of 6-Me_3-TPA (0.17 g, 0.5 mmol) in ethanol/H_2O (10 mL, 7:3 v/v) under Ar was added 0.18 g (0.5 mmol) of $Fe(ClO_4)_2$·$6H_2O$. This solution was then cooled to −40 °C using a cold bath, and *t*-BuOOH (0.3 mL, 90% in H_2O) was added dropwise. The light yellow solution immediately turned dark red, and upon standing at −40 °C for 2−3 days a red solid precipitated. This solid (water sensitive at room temperature) was collected by filtration and vacuum-dried at −40 °C. Recrystallization at room temperature from dry CH_3CN/THF gave dark red needle crystals suitable for X-ray diffraction. Anal. Calcd for **2c**·THF·$2H_2O$ ($C_{46}H_{61}Cl_3Fe_2N_8O_{17}$): C, 45.43; H, 5.02; N, 9.22; Cl, 8.75. Found: C, 45.60; H, 5.08; N, 9.23; Cl, 9.05.

[Fe_2(O)$_2$(6-Me_3-TPA)$_2$](ClO_4)$_2$ (1c). [Fe_2(O)(OH)(6-Me_3-TPA)$_2$](ClO_4)$_3$ (0.05 g, 42 μmol) was dissolved in anhydrous CH_3CN (1 mL), and Et_3N (7 μL, 50 μmol) was added, turning the dark red solution brown. Addition of anhydrous THF (20 mL) afforded brown crystals suitable for X-ray diffraction in a few hours. The crystals were collected by filtration and dried under vacuum. Anal. Calcd for **1c**·2THF·$2H_2O$ ($C_{50}H_{68}Cl_2Fe_2N_8O_{14}$): C, 50.56; H, 5.73; N, 9.43. Found: C, 50.76; H, 5.60; N, 9.27.

[Fe_2(O)(OH)(4,6-Me_6-TPA)$_2$](ClO_4)$_3$ (2d) was synthesized following the method of **2c**. Anal. Calcd for **2d**·THF ($C_{52}H_{73}Cl_3Fe_2N_8O_{16}$): C, 48.63; H, 5.73; N, 8.73. Found: C, 48.80; H, 5.96; N, 8.42.

[Fe_2(O)(OH)(BQPA)$_2$](ClO_4)$_3$ (2e). Equimolar amounts of $Fe(ClO_4)_3$·$10H_2O$ (0.53 g, 1 mmol) and BQPA (0.39 g, 1 mmol) were dissolved in methanol (10 mL). One equivalent of Et_3N (138 μL, 1 mmol) was then added to the red brown solution while stirring. After the solution was left to stand overnight at 4 °C, a red brown powder precipitated and was collected by filtration and dried under vacuum. Recrystallization from CH_3CN/THF afforded red brown crystals suitable for X-ray diffraction. Anal. Calcd for **2e**·CH_3CN ($C_{54}H_{48}Cl_3Fe_2N_9O_{14}$): C, 51.27; H, 3.82; N, 9.96. Found: C, 51.74; H, 3.60; N, 9.87.

[Fe_2(O)(OH)(BPEEN)$_2$](ClO_4)$_3$ (2f). Equimolar amounts of $Fe(ClO_4)_3$·$10H_2O$ (0.53 g, 1 mmol) and BPEEN (0.3 g, 1 mmol) were dissolved in ethanol/water (10 mL, 1:1 v/v). A 10% NaOH solution (0.4 mL, 1 equiv) was then added dropwise to this red brown solution while stirring. After the solution was left to stand overnight at 4 °C, a red powder precipitated and was filtered and dried under vacuum. Recrystallization from CH_3CN/THF afforded dark red crystals suitable for X-ray diffraction. Anal. Calcd for **2f** ($C_{36}H_{53}Cl_3Fe_2N_8O_{14}$): C, 41.59; H, 5.10; N, 10.78. Found: C, 41.80; H, 4.96; N, 10.80.

[Fe_2(O)(OH)(BPMEN)$_2$](ClO_4)$_3$ (2g) was synthesized following the method of **2f**.

[Fe_2(O)(H_3O_2)(TPA)$_2$](ClO_4)$_3$ (5a) and **[Fe_2(O)(H_3O_2)(5-Et_3-TPA)$_2$](ClO_4)$_3$ (5b)** were synthesized according to published procedures.[17]

[Fe_3(O)$_3$(5-Et_3-TPA)$_3$](ClO_4)(BPh_4)$_2$ (7b). Equimolar amounts of $Fe(ClO_4)_3$·$10H_2O$ (0.53 g, 1 mmol) and 5-Et_3-TPA (0.37 g, 1 mmol) were dissolved in MeOH (10 mL). Five equivalents of Et_3N (0.69 mL, 5 mmol) was then added to this solution. After being stirred overnight at room temperature, the solution was filtered to remove some insoluble residue. To the filtrate was added 10 equiv of $NaClO_4$ (0.68 g, 10 mmol) in H_2O (8 mL). After the solution was left to stand at 4 °C for 4 days, a brown solid was obtained which was filtered and dried under vacuum. The BPh_4 salt of this complex was obtained by dissolution of this solid (0.21 g) in CH_3CN (5 mL) solution and addition of 3 equiv of $NaBPh_4$ (0.13 g) in CH_3CN (5 mL). Vapor diffusion of ether into this solution yielded brown crystals suitable for X-ray diffraction. Anal. Calcd for **7b**·$2CH_3CN$ ($C_{124}H_{130}B_2ClFe_3N_{14}O_7$): C, 69.17; H, 6.04; N, 9.11. Found: C, 68.80; H, 5.96; N, 9.31.

Crystallographic Studies. Crystals of the complexes **1c**, **2c**, **2e**, **2f**, and **7b** were mounted onto glass fibers. For [Fe_2(O)$_2$(6-Me_3-TPA)$_2$](ClO_4)$_2$ (**1c**) and [Fe_2(O)(OH)(6-Me_3-TPA)$_2$](ClO_4)$_3$ (**2c**), data were collected at −100 °C on an Enraf-Nonius CAD-4 diffractometer with graphite-monochromated Mo Kα (λ = 0.710 69 Å) radiation. Cell constants and orientation matrixes for data collection were obtained from a least-squares refinement using the setting angles of 22 carefully centered reflections (2θ = 20.00°−43.00°) for **1c**, and 40 reflections (2θ = 12.00°−16.00°) for **2c**. The intensities of three representative reflections were measured (every 70 min of X-ray exposure time for **1c** and **2c**) throughout the data collection to ascertain crystal integrity; no decay in intensity was observed. All data were corrected for empirical absorption and Lorentz and polarization effects. All calculations were performed using an SGI INDY R4400-SC or a Pentium computer with the SHELXTL-Plus V5.0 program suite.[28] Pertinent crystallographic data and experimental conditions are summarized in Table 1. Both structures were solved by direct methods.[29] All non-hydrogen atoms were refined anisotropically, and hydrogen atoms were placed in ideal positions and refined as riding atoms with individual (or group if appropriate) isotropic displacement parameters. Selected bond lengths and bond angles are listed in Table 2.

For [Fe_2(O)(OH)(BQPA)$_2$](ClO_4)$_3$ (**2e**), [Fe_2(O)(OH)(BPEEN)$_2$](ClO_4)$_3$ (**2f**), and [Fe_3(O)$_3$(5-Et_3-TPA)$_3$](ClO_4)(BPh_4)$_2$ (**7b**), data were collected at −100 °C on a Siemens SMART system equipped with graphite-monochromated Mo Kα (λ = 0.710 73 Å) radiation and a CCD detector. An initial set of cell constants was calculated from reflections harvested from three sets of 20−30 frames. These initial sets of frames were oriented such that orthogonal wedges of reciprocal space were surveyed. Final cell constants were calculated from a set that did not

(28) SHELXTL-Plus V5.0, Siemens Industrial Automation, Inc., Madison, WI.

(29) Gilmore, C. J. *J. Appl. Crystallogr.* **1984**, *17*, 42−46.

Table 2. Selected Bond Lengths (Å) and Bond Angles (deg) for **1c**, **2c**, **2e**, and **2f**

	1c	**2c**		**2e**	**2f**	
	Fe1	Fe1 (molecule A)	Fe1 (molecule B)	Fe1	Fe1	Fe2
Fe−O	1.844(3) (O1)	1.890(7) (O1A)	1.895(10) (O1B′)	1.897(3) (O1A)	1.850(3) (O2)	1.846(3) (O2)
	1.916(4) (O1′)	1.975(7) (O1A′)	1.960(8) (O1B)	1.942(3) (O1)	1.976(4) (O1)	1.993(4) (O1)
Fe−N(in-plane)	2.194(4) (N1)	2.161(7) (N1A)	2.158(11) (N1B)	2.196(4) (N1)	2.161(4) (N1A)	2.156(4) (N1B)
	2.244(4) (N21)	2.204(7) (N21A)	2.254(9) (N21B)	2.208(4) (N3)	2.159(4) (N4A)	2.163(4) (N4B)
Fe−N(out-of-plane)	2.279(4) (N11)	2.194(7) (N11A)	2.197(1) (N11B)	2.203(4) (N4)	2.191(5) (N2A)	2.204(4) (N2B)
	2.255(4) (N31)	2.247(7) (N31A)	2.179(8) (N31B)	2.143(4) (N2)	2.269(4) (N3A)	2.266(4) (N3B)
Fe−Fe	2.716(2)	2.948(3)	2.936(3)	2.8926(9)	2.835(1)	
Fe−O−Fe	92.5(2)	99.4(3)	99.2(5)	97.8(2)	100.2(2)	91.1(2) (Fe−OH−Fe)

Table 3. Selected Bond Lengths (Å) and Bond Angles (deg) for $[Fe_3(O)_3(5\text{-}Et_3\text{-}TPA)_3](BPh_4)_2(ClO_4)$ (**7b**)

	Fe1	Fe2	Fe3
Fe−O	1.826(3) (O13)	1.825(3) (O12)	1.830(3) (O23)
	1.851(3) (O12)	1.859(3) (O23)	1.841(3) (O13)
$Fe-N_{amine}$	2.293(4) (N1)	2.330(4) (N2)	2.297(8) (N3)
$Fe-N_{py}$	2.282(4) (N13)	2.315(4) (N21)	2.284(8) (N31)
	2.212(5) (N11)	2.179(4) (N22)	2.197(5) (N32)
	2.192(4) (N12)	2.179(4) (N23)	2.180(4) (N33)
Fe−Fe	3.368 (Fe1−Fe2)	3.373 (Fe2−Fe3)	3.370 (Fe3−Fe1)
Fe−O−Fe	132.8(2)	132.6(2)	133.3(2)

exceed a number equal to 4575, 8192, and 10 192 strong reflections from the actual data collection for **2e**, **2f**, and **7b**, respectively. All calculations were performed using an SGI INDY R4400-SC or a Pentium computer with the SHELXTL-Plus V5.0 program suite.[28] Pertinent crystallographic data and experimental conditions are summarized in Table 1. All three structures were solved by direct methods.[29] All non-hydrogen atoms were refined anisotropically, and hydrogen atoms were placed in ideal positions and refined as riding atoms with individual (or group if appropriate) isotropic displacement parameters. The bridging hydroxyl proton of **2f** was not found in the difference map. Rather, it was placed at half-occupancy on two possible sites that are hydrogen bonded to two oxygen atoms of a perchlorate ion, respectively. The absolute configuration was positively determined. Selected bond lengths and bond angles are listed in Tables 2 and 3. Complete listings of bond lengths and angles and thermal and positional parameters of complexes **1c**, **2c**, **2e**, **2f**, and **7** are included in the Supporting Information.

Physical Methods. Magnetic susceptibility data were recorded on a Quantum Design SQUID susceptometer. Calibration and operation procedures have been reported elsewhere.[17,22] The data for **1c**, **2c**, and **2f** were collected over a temperature range of 10−300 K at a magnetic field of 0.5 T and were corrected for diamagnetism using Pascal's constants. Least-squares fits of the experimental data were carried out using the Heisenberg−Dirac−van Vleck Hamiltonian ($\mathbf{H} = J\mathbf{S}_1\cdot\mathbf{S}_2$) model with $S_1 = S_2 = {}^5/_2$.[30] These fits are shown in Figures S6 and S7 in the Supporting Information. ^{1}H NMR spectra were recorded on a Varian Unity 300 or 500 spectrometer at ambient temperature. Chemical shifts (in ppm) were referenced to the residual protic solvent peaks.

UV−vis spectra were recorded on a Hewlett-Packard 8452 or 8453 diode array spectrophotometer. Spectrophotometric titrations of complexes **2** were performed by adding an appropriate base (B) such as 2,4-lutidine to acetonitrile solutions of the metal complexes. The pK_a values were determined by following the change in absorbance at λ_{max} for the starting complexes (e.g., 550 nm, $\epsilon = 780$ M^{-1} cm^{-1} for **2c**). The pK_a values were calculated by using eq 1:

$$K_a(\text{complex}) = K_a(HB^+)K_{eq} \quad (1)$$

where $K_a(\text{complex}) = [H^+][Fe_2(\mu\text{-}O)_2]/[Fe_2(\mu\text{-}O)(\mu\text{-}OH)]$, $K_a(HB^+)$ was from the reported pK_a of the conjugate acid HB^+ in acetonitrile (e.g., pK_a = 14.05 for 2,4-lutidine),[31] and K_{eq} (=$[HB^+][Fe_2(\mu\text{-}O)_2]/[B][Fe_2(\mu\text{-}O)(\mu\text{-}OH)]$) was determined spectrophotometrically.

(30) O'Connor, C. J. *Prog. Inorg. Chem.* **1979**, *29*, 204−283.

(31) Izutsu, K. *Acid−base Dissociation Constants in Dipolar Aprotic Solvents*; Blackwell Scientific Publications: Brookline Village, MA, 1990; Vol. 35, p 166.

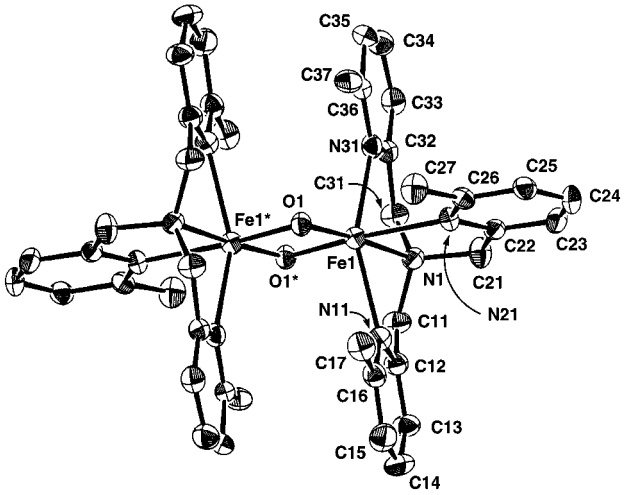

Figure 1. Representation of the X-ray crystal structure of the cation of **1c**, showing 50% probability thermal ellipsoids. Hydrogen atoms are not included for clarity.

Resonance Raman spectra were collected on an ACTON AM-506M3 monochromator with a Princeton LN/CCD data collection system using Spectra-Physics models 2030-15 argon ion and 375B CW dye (Rhodamine 6G) lasers. Low-temperature spectra of **1** and **2** in CH_3CN were obtained at 77 K using a 135° backscattering geometry. Samples were frozen onto a gold-plated copper coldfinger in thermal contact with a dewar containing liquid nitrogen. Room-temperature solution (CH_3CN) spectra of **5** were collected in a spinning cell using a 90° scattering geometry. Raman frequencies were referenced to the features of indene. Slits were set for a band-pass of 4 cm^{-1} for all spectra.

Results and Discussion

Structural Properties of the Complexes Containing Fe_2O_2-(H) Diamond Core. Complexes **1** and **2** all contain the Fe_2O_2-(H) diamond core motif with a tetradentate ligand completing the distorted octahedral environment of each iron center. As exemplified by $[Fe_2(\mu\text{-}O)_2(6\text{-}Me_3\text{-}TPA)_2](ClO_4)_2$ (**1c**) (Figure 1), this diamond core motif is characterized by a short Fe−Fe distance (less than 3 Å) and acute Fe−O−Fe angles (ca. 90°). Complex **1c** is thus far the only crystallographically characterized complex having a bis(μ-oxo)diiron(III) core. The presence of a centrosymmetric $Fe_2(\mu\text{-}O)_2$ rhomb endows **1c** with unique structural features and distinguishes it from the many diiron-(III) complexes with a single oxo bridge.[32] First, the Fe−μ-O bonds of **1c** are longer than those of (μ-oxo)diiron(III) complexes (range 1.73−1.83 Å):[32] 1.841(4) Å for Fe1−O1, which is trans to the amine nitrogen of 6-Me_3-TPA, and 1.916(4) Å for Fe1−O1′, which is trans to one of the pyridines. We attribute the lengthening of the Fe−μ-O bonds to the presence of a second oxo bridge that mitigates the Lewis acidity of the iron centers

(32) Kurtz, D. M., Jr. *Chem. Rev.* **1990**, *90*, 585−606.

and introduces significant steric constraints. A similar M−μ-O bond lengthening has also been observed for $[Mn^{III}_2(\mu\text{-O})_2]$ complexes (average 1.84 Å)[33] relative to their $[Mn^{III}_2(\mu\text{-O})]$ counterparts (average 1.79 Å).[34] Second, the Fe−O−Fe angles of 92.5(2)° are the smallest of the (μ-oxo)diiron(III) complexes, enforced by the presence of the second oxo bridge. Third, the oxo bridges of **1c** have a significant asymmetry ($\Delta r = 0.076$ Å); this asymmetry may be an intrinsic feature of the Fe_2O_2 rhomb, as suggested from a comparison with $Fe_2(\mu\text{-OH})_2$ and $Fe_2(\mu\text{-OR})_2$ complexes, which have comparable Δr values.[35] In contrast, $[Mn^{III}_2(\mu\text{-O})_2]$ and $[Cu^{III}_2(\mu\text{-O})_2]$ complexes do not exhibit such pronounced asymmetry.[16,33] Last, the Fe−Fe separation of 2.714(2) Å is the smallest separation observed for a (μ-oxo)diiron(III) unit, but it is comparable to those observed for $[Mn_2(\mu\text{-O})_2]^{n+}$ ($n = 2, 3, 4$)[36] and $[Cu_2(\mu\text{-O})_2]^{2+}$ complexes.[16]

As noted previously, the coordination environments of the iron centers in **1c** are completed by the tetradentate tripodal ligand 6-Me$_3$-TPA. The amine N and one pyridine coordinate trans to the oxo bridges to form an FeN_2O_2 plane, with the remaining two pyridines occupying axial positions. The average Fe−N_{py} bond length (2.26 Å) is ca. 0.11 Å longer than those found in (μ-oxo)diiron(III) TPA complexes[37] but typical of complexes with a pyridine having a 6-methyl substituent.[24] The 6-methyl group on the pyridine exerts steric effects that prevent the pyridine nitrogen from approaching the iron center too closely. As partial compensation, the Fe−N_{amine} bond length (2.18 Å) is 0.05 Å shorter than those in TPA complexes.[37]

Complex **2c**, the conjugate acid of **1c**, is a (μ-oxo)(μ-hydroxo)diiron(III) complex. The presence of the proton in the formulation is supported by the presence of three perchlorate anions associated with each dinuclear unit and electrospray mass spectral data.[23] The crystal structure of **2c** reveals two unique molecules per asymmetric unit, each with an inversion center located at the center of the Fe_2O_2 core (see Supporting Information). As a consequence, the μ-hydroxo proton is disordered between the two oxo bridges. The Fe−O bonds lengths (1.890(7)−1.975(7) Å) average 1.93 Å for the two molecules in the unit cell. Such bond lengths border on the short end of the range found for bis(μ-hydroxo)diiron(III) complexes (1.96−2.06 Å)[35] and are likely a compromise between the Fe−O and Fe−OH bond lengths. In agreement, EXAFS analysis[23] of **2c** shows that the presence of scatterers at 1.82 and 1.99 Å, corresponding to the Fe−μ-O and Fe−μ-OH bonds.[38]

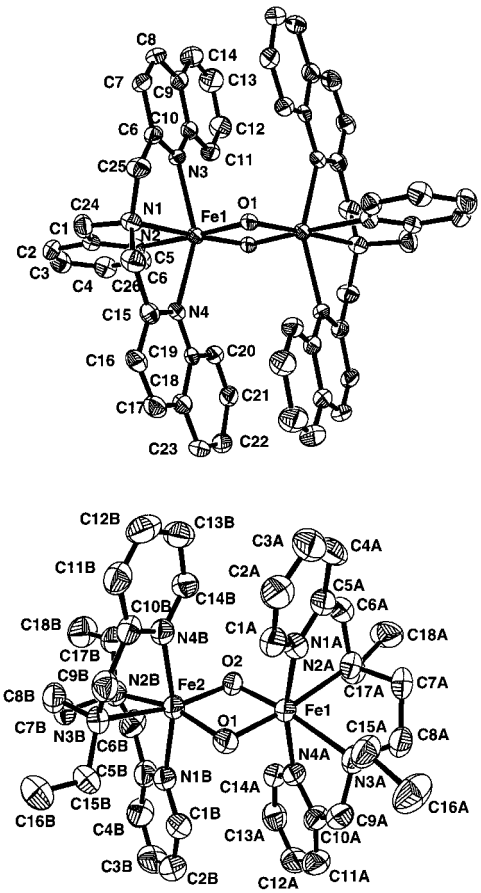

Figure 2. Representation of the X-ray crystal structure of the cation of **2e** (top) and **2f** (bottom), showing 50% probability thermal ellipsoids. Hydrogen atoms are not included for clarity.

The Fe−Fe distance for **2c** (2.94 Å) is 0.1−0.2 Å shorter than those observed for $Fe_2(\mu\text{-OH})_2$ and $Fe_2(\mu\text{-OR})_2$ complexes[35] and 0.23 Å longer than that of **1c** (Table 2). This is consistent with the increase in the average Fe−O−Fe angle to 98.7° from 92.5° in **1c**. The lengthening of the metal−metal distance upon protonation has also been observed for the series of manganese complexes $[Mn_2(\mu\text{-O})_2(\text{salpn})]$, $[Mn_2(\mu\text{-O})(\mu\text{-OH})_2(\text{salpn})]^+$, and $[Mn_2(\mu\text{-OH})_2(\text{salpn})]^{2+}$.[36] As expected, protonation of **1c** to **2c** shortens the average Fe−N bond by 0.04 Å, in agreement with the increased Lewis acidity of the iron centers in **2c**.

$[Fe_2(\mu\text{-O})(\mu\text{-OH})(\text{BQPA})_2](ClO_4)_3$ (**2e**) (Figure 2, top) has structural features extremely similar to those of $[Fe_2(\mu\text{-O})(\mu\text{-OH})(6\text{-Me}_3\text{-TPA})_2](ClO_4)_3$ (**2c**) (Table 2). The two quinoline ligands on each iron center bind trans to each other and perpendicular to the plane of the $Fe_2(\mu\text{-O})(\mu\text{-OH})$ core. The average Fe−N_{py} is 2.19 Å, 0.02 Å shorter than that of **2c**, most likely due to the smaller steric effects of the C11−H and C20−H groups on the quinoline rings compared to that of the 6-methyl substituent in 6-Me$_3$-TPA. The Fe−μ-O bonds have lengths of 1.893(3)−1.942(3) Å, averaging 1.92 Å compared to 1.94 Å in **2c**.

$[Fe_2(\mu\text{-O})(\mu\text{-OH})(\text{BPEEN})_2](ClO_4)_3$ (**2f**) is another diiron complex with a (μ-oxo)(μ-hydroxo)diiron(III) core (Figure 2, bottom).[39] The BPEEN ligand differs from 6-Me$_3$-TPA in having

(33) (a) Goodson, P. A.; Oki, A. R.; Glerup, J.; Hodgson, D. J. *J. Am. Chem. Soc.* **1990**, *112*, 6248−6254. (b) Glerup, J.; Goodson, P. A.; Hazell, A.; Hazell, R.; Hodgson, D. J.; McKenzie, C. J.; Michelsen, K.; Rychlewska, U.; Toftlund, H. *Inorg. Chem.* **1994**, *33*, 4105−4111.

(34) Wieghardt, K. *Angew. Chem., Int. Ed. Engl.* **1989**, *28*, 1153−1172.

(35) (a) Thich, J. A.; Ou, C. C.; Powers, D.; Vasiliou, B.; Mastropaolo, D.; Potenza, J. A.; Schugar, H. J. *J. Am. Chem. Soc.* **1976**, *98*, 1425−1433. (b) Borer, L.; Thalken, L.; Ceccarelli, C.; Glick, M.; Zhang, J. H.; Reiff, W. M. *Inorg. Chem.* **1983**, *22*, 1719−1724. (c) Ou, C.-C.; Lalancette, R. A.; Potenza, J. A.; Schugar, H. J. *J. Am. Chem. Soc.* **1978**, *100*, 2053−2057. (d) Ménage, S.; Que, L., Jr. *Inorg. Chem.* **1990**, *29*, 4293−4297. (e) Bertrand, J. A.; Eller, P. G. *Inorg. Chem.* **1974**, *13*, 927−934. (f) Chiari, B.; Piovesana, O.; Tarantelli, T.; Zanazzi, P. F. *Inorg. Chem.* **1982**, *21*, 2444−2448. (g) Chiari, B.; Piovesana, O.; Tarantelli, T.; Zanazzi, P. F. *Inorg. Chem.* **1984**, *23*, 3398−3404.

(36) (a) Baldwin, M. J.; Stemmler, T. L.; Riggs-Gelasco, P. J.; Kirk, M. L.; Penner-Hahn, J. E.; Pecoraro, V. L. *J. Am. Chem. Soc.* **1994**, *116*, 11349−11356. (b) Baldwin, M. J., Pecoraro, V. L. *J. Am. Chem. Soc.* **1996**, *118*, 11325−11326.

(37) (a) Yan, S.; Cox, D. D.; Pearce, L. L.; Juarez-Garcia, C.; Que, L., Jr.; Zhang, J. H.; O'Connor, C. J. *Inorg. Chem.* **1989**, *28*, 2507−2509. (b) Norman, R. E.; Holz, R. C.; Ménage, S.; O'Connor, C. J.; Zhang, J. H.; Que, L., Jr. *Inorg. Chem.* **1990**, *29*, 4629−4631. (c) Norman, R. E.; Yan, S.; Que, L., Jr.; Backes, G.; Ling, J.; Sanders-Loehr, J.; Zhang, J. H.; O'Connor, C. J. *J. Am. Chem. Soc.* **1990**, *112*, 1554−1562. (d) Holz, R. C.; Elgren, T. E.; Pearce, L. L.; Zhang, J. H.; O'Connor, C. J.; Que, L., Jr. *Inorg. Chem.* **1993**, *32*, 5844−5850.

(38) This technique provides a radial distribution of scatterers about the metal center, so the metal−ligand distances obtained by EXAFS would be unaffected by the disorder imposed by the symmetry of the unit cell.

(39) The related BPMEN complex reported by Toflund and co-workers has not been characterized crystallographically (see ref 41).

Table 4. Structural Parameters of the Diiron Cores for All Relevant Complexes

structure motif	ligands	Fe−μ-O (Å)	Fe−OH (Å)	Fe−OH_2 (Å)	Fe−Fe (Å)	Fe−μ-O−Fe (deg)
$Fe_2(\mu\text{-O})(H_2O)_2$	TPA[17]	1.78, 1.79		2.09, 2.14	3.57	174.1
$Fe_2(\mu\text{-O})(\mu\text{-}H_3O_2)$	TPA[17,48]	1.78, 1.84	1.91	2.04	3.39	138.9
	5-Et_3-TPA[17]	1.78, 1.83	1.91	2.05	3.35	136.3
	BPMEN[40]	1.82, 1.83	1.99	2.05	3.40	137.5
$Fe_2(\mu\text{-O})(\mu\text{-OH})$	6-Me_3-TPA	1.82[a]	1.99[a]	2.95		
	BQPA	*b*	*b*		2.89	
	BPEEN	1.85	1.99		2.84	100.2
$Fe_2(\mu\text{-O})_2$	6-Me_3-TPA	1.84, 1.92			2.71	92.5
$Fe_3(\mu\text{-O})_3$	5-Et_3-TPA	1.84[c]			3.37	132.9

[a] Data are taken from EXAFS studies. [b] Fe−O distances are not shown due to their mixing with Fe−OH distances induced by the disorder in the crystal structures. [c] 1.84 Å is the average distance for six Fe−O bonds.

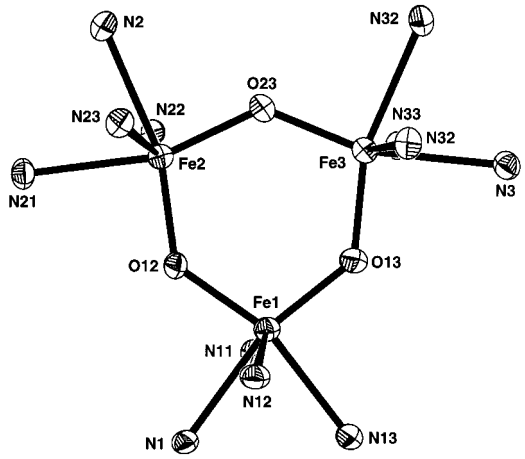

Figure 3. Representation of the core structure of **7b**, showing 50% probability thermal ellipsoids.

two pyridyl and two amine donors. In this complex, both amine nitrogens coordinate trans to the two bridging oxygens. In contrast to **2c**, the $Fe_2(\mu\text{-O})(\mu\text{-OH})$ core of this complex is not disordered. The hydroxide proton is hydrogen bonded to a perchlorate ion, thereby fixing the proton on one of the oxygen bridges. The Fe−μ-O bonds (1.85 Å) are comparable to the shorter Fe−μ-O bond in **1c** (1.841(4) Å), while the Fe−μ-OH bonds (1.98 Å) are similar to the Fe−μ-OH bond length (1.99 Å) determined for **2c** by EXAFS.[23] This $Fe_2(\mu\text{-O})(\mu\text{-OH})$ core gives rise to an Fe−O−Fe angle of 100.2(2)°, an Fe−(OH)−Fe angle of 91.1(2)°, and an Fe−Fe distance of 2.835(1) Å.

Our attempt to obtain a bis(μ-oxo)diiron(III) complex with 5-Et_3-TPA by reaction of $[Fe_2(\mu\text{-O})(5\text{-}Et_3\text{-TPA})_2(\mu\text{-}H_3O_2)]^{3+}$ (**5b**) with 1 equiv of base yielded the first example of a tris(μ-oxo)triiron(III) complex, $[Fe_3(\mu\text{-O})_3(5\text{-}Et_3\text{-TPA})_3]^{3+}$ (**7b**, Figure 3 and Table 3). Complex **7b** has a nearly planar six-membered Fe_3O_3 ring with alternating iron and oxygen atoms. The oxygen atoms deviate from the plane defined by the three iron atoms by no more than ±0.01 Å, and the ring torsion angles are all less than 8°. The Fe−O−Fe angles average 132.9°, while the O−Fe−O angles average 107°, resulting in Fe−Fe distances of approximately 3.37 Å. The metal−ligand geometry is as expected from a comparison with other (μ-oxo)diiron(III) TPA complexes.[37] The Fe−μ-O bonds trans to an amine nitrogen (average 1.83 Å) are 0.02 Å shorter than those trans to a pyridine (average 1.85 Å), while the Fe−N_{py} bonds trans to the oxo bridges (average 2.29 Å) are 0.1 Å longer than the other Fe−N_{py} bonds (average 2.19 Å).

With the complexes discussed above, we now have a collection of related structures of (μ-oxo)diiron(III) complexes that have additional water-derived ligands in different ionization states (Scheme 1). Metric parameters of the diiron cores for all relevant complexes are compiled and compared in Table 4. A perusal of this table shows that the Fe−μ-O bond length is quite sensitive to the ionization state of the additional water-derived ligand, lengthening from 1.78−1.79 Å for an iron(III) center with an additional aqua ligand (e.g., **6**) to a range of 1.83−1.84 Å for an iron(III) center with an additional hydroxide (or its equivalent) (e.g., **5** and **7b**). These changes reflect the decreased Lewis acidity of the iron(III) center. The Fe−μ-O bond further lengthens upon formation of the Fe_2O_2 rhomb, as shown by comparing the values for the BPMEN complex with an additional H_3O_2 bridge (average 1.82 Å)[40] versus the BPEEN complex with an additional hydroxyl bridge (1.85 Å). Similarly, the average Fe−O bond length in **7b** (1.84 Å) is 0.04 Å shorter than that for **1c** (1.88 Å). Presumably, the bond lengthening reflects the steric strain of forming a four-membered Fe_2O_2 ring.

Magnetic Properties of the Fe_2O_2(H) Diamond Core. The temperature dependence of the magnetic susceptibilities of solid samples of **1c** and **2c** is best fit with $J = +54(8)$ and $+113(10)$ cm^{-1} ($\mathbf{H} = J\mathbf{S}_1\cdot\mathbf{S}_2$), respectively.[22] Data for the BPEEN complex **2f** have also been obtained (see Supporting Information) and fit with $J = +106(10)$ cm^{-1}. This value matches that of the related **2c** well but is significantly larger than the *J* value reported by Toftlund and co-workers for the corresponding BPMEN complex **2g**.[41,42] Complexes **1** and **2** exhibit significantly smaller *J* values than those reported for (μ-oxo)diiron(III) complexes (range from 180 to 250 cm^{-1}),[32] an observation which belies expectations of stronger coupling due to the presence of two efficient exchange pathways. It has been noted that *J* is not very sensitive to the Fe−O−Fe angle in the range of 120°−180°, because of the opposing angular dependences of the many pairwise interactions between the magnetic orbitals of the two $S = {}^5/_2$ ions.[43] However, the diamond core structures of **1c**, **2c**, and **2f** have Fe−O−Fe angles between 90° and 100° and longer Fe−μ-O bonds, points not previously available in the magnetostructural correlations. Gorun and Lippard have proposed that the *J* value reflects essentially the exchange pathway through the oxo bridge and should depend on the Fe−μ-O bond lengths according to the relationship $J = A\exp(BP)$, where *P* is defined as half of the shortest superexchange pathway between two iron(III) ions (*A* and *B* are the fitting constants).[44] Indeed, the availability of complexes such as **1** and **2** validates and refines this correlation by providing needed values for intermediate Fe−O−Fe lengths. The *J* values for **2c** and **2f** ($P = 1.85$ Å for both **2c** and **2f** using the average of the two Fe−

(40) Poussereau, S.; Blondin, G.; Cesario, M.; Guilhem, J.; Chottard, G.; Gonnet, F.; Girerd, J.-J. *Inorg. Chem.* **1998**, *37*, 3127−3132.

(41) Hazell, R.; Jensen, K. B.; McKenzie, C. J.; Toftlund, H. *J. Chem. Soc., Dalton Trans.* **1995**, 707−717.

(42) Complex **2g** was reported to have $J = 84$ cm^{-1}, but the authors mentioned their dissatisfaction with the fit they obtained.[41]

(43) Hotzelmann, R.; Wieghardt, K.; Flörke, U.; Haupt, H.-J.; Weatherburn, D. C.; Bonvoisin, J.; Blondin, G.; Girerd, J.-J. *J. Am. Chem. Soc.* **1992**, *114*, 1681−1696.

(44) Gorun, S. M.; Lippard, S. J. *Inorg. Chem.* **1991**, *30*, 1625−1630.

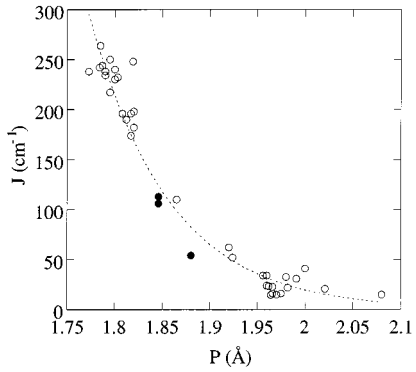

Figure 4. Plot of J ($\mathbf{H} = J\mathbf{S}_1\cdot\mathbf{S}_2$) vs P (P is one-half of the shortest superexchange pathway between two iron(III) ions). The open circles represent data from ref 43 and references therein, and the line represents the equation ($J = A\exp(BP)$, where $A = 17.52$, $B = -12.663$). The solid circles are the experimental data for **1c**, **2c**, and **2f** (P for **2c** is assumed to be the same as that for **2f**).

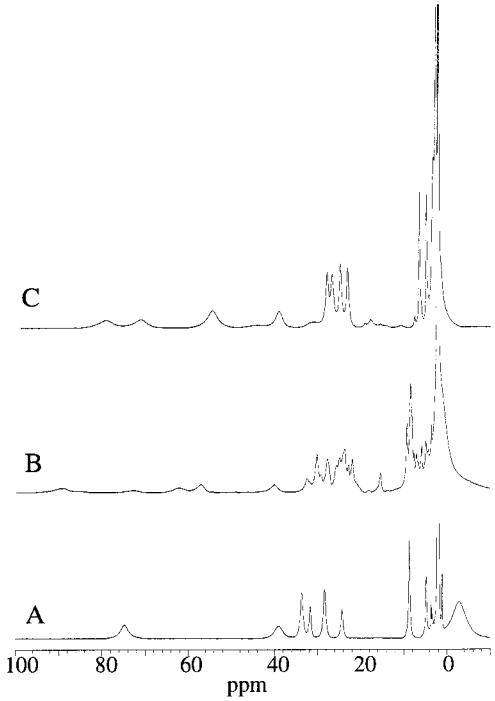

Figure 5. ^{1}H NMR spectra of (A) **1c**, (B) **2c**, and (C) **2f** recorded in CD_3CN.

μ-O bonds of **2f**) fit well onto the line derived from Gorun and Lippard's relationship (Figure 4),[46] but that of **1c** is somewhat lower than predicted ($J = 80$ cm^{-1} for $P = 1.88$). Using the method of Weihe and Güdel[45] does not yield an improved agreement, $J = 100$ cm^{-1} for **2f** and $J = 80$ cm^{-1} for **1c**. Since **1** and **2** represent the first (μ-oxo)diiron(III) complexes with such acute Fe−O−Fe angles, it is likely that these smaller angles also play a role in the weakening of the antiferromagnetic interaction.

The ^{1}H NMR spectra of **1c**, **2c**, and **2f** (Figure 5) indicate that the solid-state structures persist in solution. Unlike the strongly antiferromagneticaly coupled (μ-oxo)diiron(III) complexes (**5** and **6**) with peaks from 0 to +35 ppm,[17] **1** and **2** show peaks paramagnetically shifted over a range from −5 to +90 ppm, the wider range of paramagnetic shifts consistent with the weaker antiferromagnetic interactions between the iron centers. Previous studies on iron complexes with these ligands indicated that the β protons of the pyridine rings of the ligands are very sensitive to the electronic properties of the iron centers.[24,37] These protons are found at 24−34 ppm in the spectrum of **1c** and at 23−30 ppm for **2c**. The more paramagnetically shifted β protons of **1c** are consistent with the magnetization results, showing a weaker antiferromagnetic interaction for **1c**.

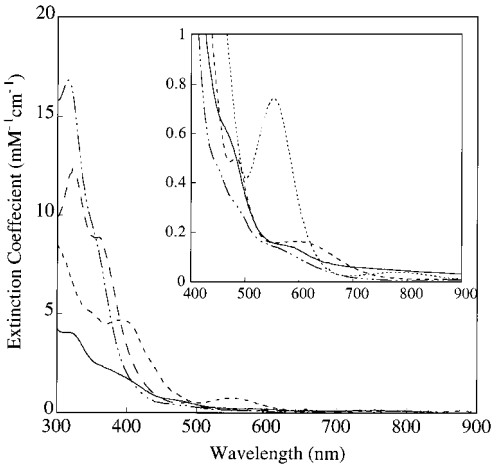

Figure 6. UV−vis spectra of **1c** (—), **2c** (- - -), and **6a** (—···—) in CH_3CN and **5a** (— — —) in CH_3CN in the presence of 1000 equiv of H_2O. The inset is the expanded region of 400−900 nm.

UV−Vis Properties of Fe_2O_2(H) Complexes: Acid−Base and Aquation Equilibria. Complexes containing the Fe_2O_2(H) diamond core have UV−vis absorption properties (Figure 6 and Table 5) distinct from those of any other (μ-oxo)diiron(III) complexes due to their acute Fe−O−Fe angles. Bands of [$Fe_2(\mu$-O)$(TPA)_2$] complexes in the 600−700-nm region have been assigned to have oxo-to-iron(III) charge-transfer character and are indicative of the Fe−O−Fe angle.[37b,d] Such bands red shift as the Fe−O−Fe angle decreases. The corresponding feature for complexes **2c**−**g** is a weak broad band at ca. 800 nm. The considerable red shift of this band, compared to the λ_{max} assigned for this transition for other (μ-oxo)diiron(III) complexes (600−700 nm, corresponding to Fe−O−Fe angles of 140°−120°)[37] is consistent with a much more acute Fe−O−Fe angle (ca. 100°). The ca. 550-nm band of **2c**−**g** is assigned to one of the bands usually observed in the 400−530-nm region of the electronic spectra of multiply bridged (μ-oxo)diiron(III) complexes, which red shifts and/or gains intensity as the Fe−O−Fe angle decreases.[37] The red shift to 550 nm is again consistent with the considerable decrease of the Fe−O−Fe angle.

The corresponding visible absorption features of **1c** are found at 760 and 470 nm. Though considerably red shifted when compared to those of other (μ-oxo)diiron(III) complexes, these values are blue shifted relative to those of **2c,** despite the smaller Fe−O−Fe angles of **1c** (92.5° vs ∼100°). This apparent anomaly may be due to the change on the charge of the bridging ligand. The second μ-oxo bridge in **1c** decreases the Lewis acidity of the iron atoms, thereby widening the gap between the ligand donor and the iron acceptor orbitals and resulting in a blue shift.

Addition of 1 equiv of Et_3N to CH_3CN solutions of $Fe_2(\mu$-O)(μ-OH) complexes (**2**) converts them to complexes with $Fe_2(\mu$-O)$_2$ cores, as revealed by the disappearance of the ca. 550-nm band and its replacement by the ca. 470-nm band which is

(45) Weihe, H.; Güdel, H. U. *J. Am. Chem. Soc.* **1998**, *120*, 2870−2879.
(46) The definition we use here is $\mathbf{H} = J\mathbf{S}_1\cdot\mathbf{S}_2$ instead of $\mathbf{H} = -2J\mathbf{S}_1\cdot\mathbf{S}_2$ as used in Gorun and Lippard's paper; therefore, $A = 17.52$ and $B = -12.663$ were used in the equation to generate the line.

Table 5. UV−Vis Properties and pK_a Values of Fe_2O_2(H)-Containing and Related Complexes

	1c	2c	2d	2e	2f	2g	2a	2b	5a	5b	5f	7
λ, nm	760	800	800	800	790	790	800	800	610	605	650	604
(ϵ, mM^{-1} cm^{-1})	(0.08)[a]	(0.07)	(0.07)	(0.06)	(0.08)	(0.07)	(0.08)	(0.08)	(0.16)	(0.20)		(0.38)
	470	550	554	554	558	555	558	554	480	485	480	530
	(0.56)	(0.78)	(0.70)	(0.79)	(0.80)	(0.70)	(0.30)	(0.52)	(0.50)	(0.50)		(0.51)
					510	512	494					490
					(0.56)	(0.54)	(0.45)					(0.48)
					475	479						
					(0.65)	(0.65)						
					430	430						
					(2.0)	(2.07)						
	375	396	400	396	378	377			360	360	365	
	(2.0)	(4.7)	(4.0)	(4.5)	(4.8)	(4.7)			(10)	(11)		
	320	340		308					322		320	320
	(4.2)	(5.0)		(17)					(16)		(16)	(2.0)
pK_a		15.9	16.3	17.6	17.0	16.9						

characteristic of the $Fe_2(\mu\text{-O})_2$ core. This conversion is also confirmed by the appearance of NMR features of the more weakly coupled **1**, as discussed in the previous section. While **1c** (and presumably **1d**) can be isolated as a solid, attempts to obtain the conjugate bases of **2a**, **2b**, **2e**, **2f**, and **2g** as solids afforded the corresponding tris(μ_2-oxo)triiron complexes exemplified by **7b**. Such species have absorption features at 490 (ϵ = 480 M^{-1} cm^{-1}), 532 (ϵ = 510 M^{-1} cm^{-1}), and 604 nm (ϵ = 380 M^{-1} cm^{-1}), associated with Fe−O−Fe angles around 130°. For **2a**, **2b**, **2e**, **2f**, and **2g**, the initially formed $Fe_2(\mu\text{-O})_2$ cores may be in equilibrium with small amounts of the corresponding $Fe_2(\mu\text{-O})(OH)_2$ cores (**4**) (Scheme 1), which then rapidly convert to thermodynamically more stable trinuclear complexes upon precipitation.

The pK_a's of the μ-OH protons of **2** can be determined by spectrophotometric titrations. Acetonitrile was selected as the standard solvent because of the good solubility of the complexes and the availability of a number of organic bases for which pK_a's have been reported in this solvent.[31] The titration of **2c** with 2,4-lutidine is illustrated in Figure 7 (top), and the pK_a's are listed in Table 5. The pK_a values of **2a** and **2b** could not be obtained due to the rapid hydration of the solvent acetonitrile in the presence of excess base, resulting in the formation of diiron(III) acetamido complexes.[47,48] The pK_a values decrease in the series L = BQPA, BPEEN, BPMEN, 4,6-Me_6-TPA, and 6-Me_3-TPA, which we attribute to the electronic and steric effects of the ligands. Despite their electron-donating properties, the 6-methyl groups in 6-Me_3-TPA and 4,6-Me_6-TPA introduce steric hindrance and lengthen the Fe−N_{py} bonds.[24] Consequently, the iron centers in **2c** are the most Lewis acidic of the series, and the μ-OH bridge has the lowest pK_a.

The ca. 550-nm visible band characteristic of complexes with the $Fe_2(\mu\text{-O})(\mu\text{-OH})$ core has also been used to recognize an equilibrium between complexes **2** and **5** (L = TPA (**a**), 5-Et_3-TPA (**b**), BPEEN (**f**), BPMEN (**g**)) (Scheme 1). Complexes **5a** and **5b,** which have a $[Fe_2(\mu\text{-O})(\mu\text{-}H_3O_2)]^{3+}$ core structure and are green in the solid state,[17] dissolve in dry CH_3CN to afford red solutions and a visible absorption band at ca. 550 nm. Upon addition of H_2O or reduction of the temperature, the red solutions gradually turn green (Figure 7, bottom). Absorption features at 605, 485, and 360 nm, which are characteristic of a $[Fe_2(\mu\text{-O})(\mu\text{-}H_3O_2)]^{3+}$ (**5**) core,[17] become distinct with 1000 equiv of H_2O added or below −20 °C. In contrast, **2f** and **2g** are isolated as $Fe_2(\mu\text{-O})(\mu\text{-OH})$ complexes. Similarly, when H_2O is added to the red solution of **2f** or **2g** in CH_3CN, the characteristic ca. 550-nm band decreases in intensity, and new features grow in. The new features at 650 and 480 nm become distinct only after addition of a large amount of water (6000 equiv). A similar equilibrium was reported for **2g** by Poussereau et al.[40] The changes in core structures can also be monitored by resonance Raman spectroscopy, as discussed in the next section.

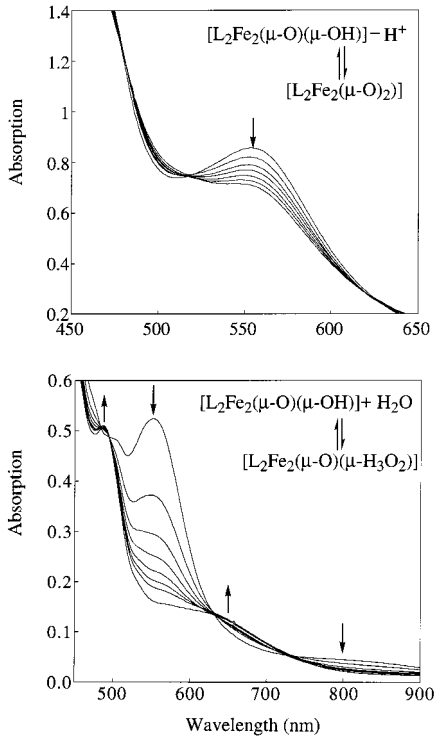

Figure 7. (Top) UV−vis spectral titration of **2c** with 2,4-lutidine in CH_3CN (25 equiv of base added per succeeding trace). (Bottom) Titration of **2b** with H_2O in CH_3CN (50 equiv of H_2O added per succeeding trace, 1000 equiv of H_2O added to the last trace).

Vibrations of the $Fe_2(\mu\text{-O})(\mu\text{-OH})$ Core: Assignment of Fe−O−Fe Modes. The complexes with an $Fe_2(\mu\text{-O})(\mu\text{-OH})$ core (**2**) exhibit vibrational properties (Figures 8 and 9, Table 6) that arise from the novel core structure. In contrast to the vibrations of complexes containing an Fe_2O_2 diamond core, which are explained in the context of a tetraatomic core,[49] vibrations of complexes **2c**−**f** instead are based on a triatomic

(47) Wilkinson, E. C.; Dong, Y.; Que, L., Jr. *J. Am. Chem. Soc.* **1994**, *116*, 8394−8395.

(48) Hazell, A.; Jensen, K. B.; McKenzie, C. J.; Toftlund, H. *Inorg. Chem.* **1994**, *33*, 3127−3134.

(49) Wilkinson, E. C.; Dong, Y.; Zang, Y.; Fujii, H.; Fraczkiewicz, R.; Fraczkiewicz, G.; Czernuszewicz, R. S.; Que, L., Jr. *J. Am. Chem. Soc.* **1998**, *120*, 955−962.

Table 6. Resonance Raman Data of Complexes Containing an $Fe_2(\mu\text{-O})(\mu\text{-OH})$ Core

	2c	2d	2e	2f	2g	2b	5b	5f
ν_{asym} (cm^{-1})[a]	675 (−30) 666 (−32)	672 (−30)	668 (−36)			676		
ν_{sym} (cm^{-1})[a]	591 (−27)	587 (−27)	600 (−25)	596 (−29)	600		462 (−12)	448 (−10)
$\nu_{Fe-OH-Fe}$ (cm^{-1})[a]		497 (−13) [−3]		504 (−7, −16) [−4]				
Fe−O−Fe angle (deg)		*b*	*b*	100.2			134	

[a] Values in parentheses are ^{18}O shifts, while those in brackets are ^{2}H shifts. [b] Fe−O−Fe angles are not shown due to the disorder in the crystal structures.

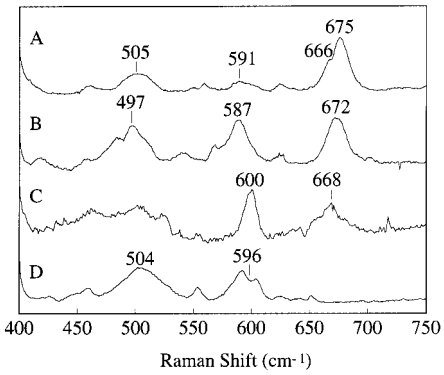

Figure 8. Resonance Raman spectra obtained with 514.5-nm excitation of frozen CH_3CN solutions of (A) $[Fe_2(\mu\text{-O})(\mu\text{-OH})(6\text{-Me}_3\text{-TPA})_2](ClO_4)_3$ (**2c**), (B) $[Fe_2(\mu\text{-O})(\mu\text{-OH})(4,6\text{-Me}_6\text{-TPA})_2](ClO_4)_3$ (**2d**), (C) $[Fe_2(\mu\text{-O})(\mu\text{-OH})(BQPA)_2](ClO_4)_3$ (**2e**), and (D) $[Fe_2(\mu\text{-O})(\mu\text{-OH})(BPEEN)_2](ClO_4)_3$ (**2f**).

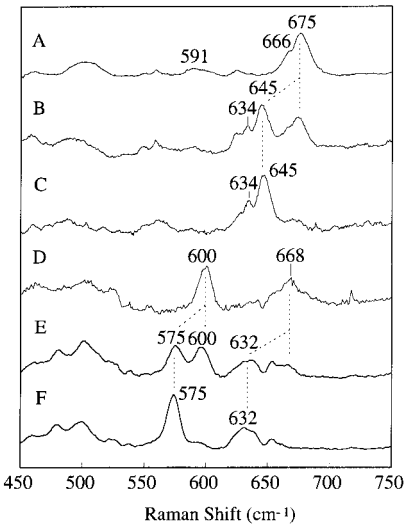

Figure 9. Resonance Raman spectra of (A) $[Fe_2(\mu\text{-O})(\mu\text{-OH})(6\text{-Me}_3\text{-TPA})_2](ClO_4)_3$ (**2c**), (B) **2c** with 300 equiv of a 1:1 mixture of $H_2{}^{16}O$:$H_2{}^{18}O$, (C) **2c** with 300 equiv of $H_2{}^{18}O$ added, (D) $[Fe_2(\mu\text{-O})(\mu\text{-OH})(BQPA)_2](ClO_4)_3$ (**2e**), (E) **2e** with 300 equiv of a 1:1 mixture of $H_2{}^{16}O$:$H_2{}^{18}O$, and (F) **2e** with 300 equiv of $H_2{}^{18}O$ added.

framework. The systematic study of Fe−O−Fe complexes by Sanders-Loehr et al.[50] serves as the basis for our analysis. In that study, the symmetric Fe−O−Fe stretching mode of the C_{2v} Fe−O−Fe unit is seen as a strong band in the resonance Raman spectrum in the region between 380 and 540 cm^{-1}, which increases in energy as the Fe−O−Fe angle decreases. The asymmetric Fe−O−Fe stretch is usually found in the infrared spectrum (and sometimes in the Raman spectrum) in the region between 720 and 870 cm^{-1}, and the energy of the vibration decreases as the Fe−O−Fe angle decreases. These correlations are illustrated in Figure 10. Complexes **2c**−**f** have ^{18}O-sensitive

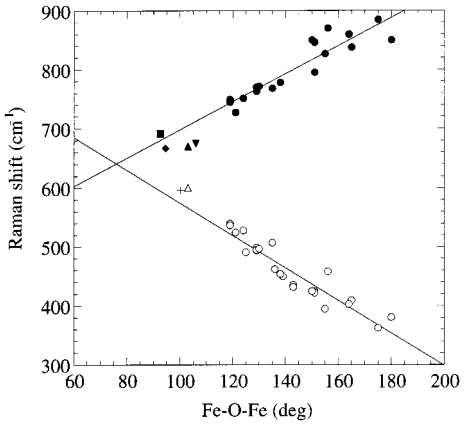

Figure 10. Plot of Fe−O−Fe angle vs ν_{sym} (○) and ν_{asym} (●) for a variety of complexes containing Fe−O−Fe cores from ref 50 and references therein. Additional data for complexes with $Fe_2(O)_2(H)$ cores are represented by ■ for the ν_{asym} of **1c**, ▼ for the ν_{asym} of **2c**, ▲ for the ν_{asym} and △ for the ν_{sym} of **2d**, and + for the ν_{sym} of **2f**. The ν_{asym} for $[Fe_2(\mu\text{-O})_2(5\text{-Me}_3\text{-TPA})_2](ClO_4)_3$ from ref 49 is represented by ◆.

bands at ca. 670 and ca. 600 cm^{-1} with differing relative intensities. Complex **2c** exhibits a strong band at 675 cm^{-1} and a shoulder at 666 cm^{-1} that undergo a ca. 30-cm^{-1} downshift after ^{18}O exchange (Figure 9C). A weak band at 591 cm^{-1} was also observed for **2c**. In contrast, **2f** exhibits no feature at ca. 670 cm^{-1} and a Fermi doublet centered at 596 cm^{-1}. Complexes **2d** and **2e**, on the other hand, exhibit both bands (Figures 8 and 9). When viewed in the context of the correlation of Sanders-Loehr et al., the ca. 600-cm^{-1} vibrations of these complexes fit nicely on the line for the ν_{sym} (Fe−O−Fe) corresponding to a complex with an Fe−O−Fe angle of 100°. The ca. 670-cm^{-1} vibrations are then associated with the corresponding ν_{asym} mode (Figure 10). The switch from a dominant ν_{asym} in **2c** to a dominant ν_{sym} in **2f** can be understood by considering the symmetry of the Fe−O−Fe unit. As noted, **2c**−**e** have one Fe−O bond trans to an amine nitrogen and the other trans to a pyridine nitrogen, which should give rise to an asymmetric Fe−O−Fe unit and result in an enhanced ν_{asym}, as observed for model complexes with unsymmetric (μ-oxo)diiron cores, such as $[N5FeOFeX_3]^+$ (X = Cl^- or Br^-)[51] and $[Fe_2O(O_2CCPh_3)_2(Me_3TACN)_2]^{2+}$.[52] On the other hand, **2f** has a symmetric Fe−O−Fe unit and an enhanced ν_{sym}.[53]

Mixed-isotope labeling experiments have been carried out to confirm that the vibrations discussed above are, indeed, triatomic Fe−O−Fe vibrations. Samples of **2c** and **2e** allowed to exchange with 300 equiv of $H_2O/H_2{}^{18}O$ (1: 1 ratio) afford resonance Raman spectra (Figure 9B and E, respectively) with two sets of bands which are associated with ^{16}O- or ^{18}O-enriched

(50) Sanders-Loehr, J.; Wheeler, W. D.; Shiemke, A. K.; Averill, B. A.; Loehr, T. M. *J. Am. Chem. Soc.* **1989**, *111*, 8084−8093.

(51) Gómez-Romero, P.; Witten, E. H.; Reiff, W. M.; Backes, G.; Sanders-Loehr, J.; Jameson, G. B. *J. Am. Chem. Soc.* **1989**, *111*, 9039−9047.

(52) Cohen, J. D.; Payne, S.; Hagen, K. S.; Sanders-Loehr, J. *J. Am. Chem. Soc.* **1997**, *119*, 2960−2961.

(53) Complex **2g** was reported to have Raman features similar to those of **2f** (ref 40).

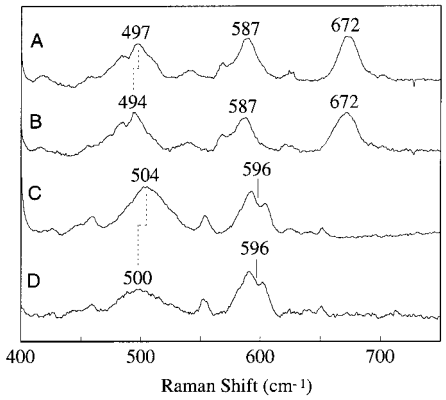

Figure 11. Resonance Raman spectra of (A) $[Fe_2(\mu\text{-}O)(\mu\text{-}OH)(4,6\text{-}Me_6\text{-}TPA)_2](ClO_4)_3$ (**2d**), (B) **2d** with 300 equiv of D_2O added, (C) $[Fe_2(\mu\text{-}O)(\mu\text{-}OH)(BPEEN)_2](ClO_4)_3$ (**2f**), and (D) **2f** first treated with 2000 equiv of D_2O and then stripped to dryness and redissolved in dry CH_3CN to effect the deuteriation of the (μ-OH) bridge.

samples, as expected for triatomic Fe−O−Fe vibration modes. No feature of intermediate energy is observed, in contrast to what has been reported for M_2O_2 complexes (M = Fe, Cu).[49,54] Thus, the possibility that these vibrations arise from modes of a tetraatomic $Fe_2(\mu\text{-}O)(\mu\text{-}OH)$ core can be excluded.

The utility of the correlations in Figure 10 is illustrated in the corroboration of an equilibrium between complexes **2** and **5** that was initially suggested by changes in the visible spectra of these complexes (vide supra). The resonance Raman spectrum of **5a** or **5b** in wet CH_3CN shows a ν_{sym} (Fe−O−Fe) at ca. 462 cm^{-1}, as expected for an Fe−O−Fe angle of 140°. In dry CH_3CN, however, this peak is replaced by a new feature at 676 cm^{-1} corresponding to the ν_{asym} of an $Fe_2(\mu\text{-}O)(\mu\text{-}OH)$ core (**2a** or **2b**). Thus, a molecule of H_2O is lost from the $Fe_2(\mu\text{-}O)(\mu\text{-}H_3O_2)$ core. Similarly, addition of 1000 equiv of H_2O to a sample of **2f** in CH_3CN results in the disappearance of the 596-cm^{-1} Fermi doublet and the appearance of a strong peak at 448 cm^{-1} (see Figure S8 in the Supporting Information). The interconversion of core structures of **2g** and **5g** was previously noted from Raman studies by Poussereau et al.[40]

Raman spectra of these $Fe_2(\mu\text{-}O)(\mu\text{-}OH)$ complexes exhibit another interesting feature at ca. 500 cm^{-1}. This vibration, most clearly observed in the spectra of **2d** and **2f** (Figure 11), is both $H_2{}^{18}O$ sensitive and ^2H_2O sensitive and thus is assigned to the Fe−(OH)−Fe vibration. In the case of **2d,** the 497-cm^{-1} band shifts to 484 cm^{-1} upon $H_2{}^{18}O$ exchange and shifts to 494 cm^{-1} upon ^2H_2O exchange. The 13-cm^{-1} shift upon labeling with ^{18}O is consistent with calculations from the secular equation for an Fe−(OH)−Fe unit.[55] However, the 3-cm^{-1} shift in ^2H_2O is smaller than expected, suggesting that this mode may not be a pure Fe−(OH)−Fe stretching vibration. No Fe−(OH)−Fe stretching frequency has been reported for (μ-hydroxo)diiron model complexes due to the lack of a visible chromophore. In this case, the observation of the $\nu_{Fe-(OH)-Fe}$ at ca. 500 cm^{-1} may be due to its coupling with the Fe−O−Fe chromophore. A Cu−(OH)−Cu stretching vibration was observed at 465 cm^{-1} by Sanders-Loehr and co-workers,[56] attributed to the coupling of the Cu−(OH)−Cu vibration to a phenolate-to-copper(II) charge-transfer band. Due to the near orthogonality of the Fe−μ-OH bonds (∠Fe−(OH)−Fe = 91.1(2)°), the Fe−(OH)−Fe vibration may be viewed as an isolated ν_{Fe-OH} mode. Indeed, ν_{Fe-OH} vibrations have been reported at ca. 500 cm^{-1} for the terminal Fe−OH units in alkaline horseradish peroxidase,[57] hydroxomethemoglobin,[58] and myoglobin.[59]

Summary and Biological Relevance

We have synthesized the first bis(μ-oxo)diiron(III) and (μ-oxo)(μ-hydroxo)diiron(III) complexes and found them to have novel structural and electronic properties. These molecules provide benchmarks with which to judge the proposition that such cores may be present in the high-valent intermediates that participate in the oxygen activation mechanisms of methane monooxygenase and related enzymes. These two core structures can be interconverted by protonation equilibria with pK_a's of 16−18 in CH_3CN. For ligands other than 6-Me_3-TPA and 4,6-Me_3-TPA, the $Fe_2(\mu\text{-}O)_2$ core cannot be isolated due to a subsequent conversion to apparently more stable $Fe_3(\mu_2\text{-}O)_3$ cores. Complexes containing $Fe_2(\mu\text{-}O)(\mu\text{-}OH)$ cores (L = TPA, 5-Et_3-TPA, BPMEN, and BPEEN) also exhibit aquation equilibria to form complexes with $Fe_2(\mu\text{-}O)(\mu\text{-}H_3O_2)$ cores. It is clear from these studies that electronic and steric properties of the ligands significantly affect the various equilibria, demonstrating a rich chemistry involving water-derived ligands alone. The significantly acute Fe−O−Fe angles enforced by the $Fe_2O_2(H)$ core endow the complexes with UV−vis, Raman, and magnetic properties quite distinct from those of the more common (μ-oxo)diiron(III) derivatives. These spectroscopic signatures can thus serve as useful tools to ascertain the presence of such core structures in metalloenzyme active sites.

Germane to the reactivity of the $M_2(\mu\text{-}O)_2$ cores is their protonation. The modulation of the core redox potentials of synthetic $Mn_2(\mu\text{-}O)_2$ complexes by protonation has led to the proposal that the different configurations of the S_1 and S_2 states and *S*-state advancement may be controlled by protonation state changes.[36] Analogous effects may control the oxidative properties of the putative $Fe_2(\mu\text{-}O)_2$ cores of intermediate **Q** of MMO and intermediate **X** of RNR R2. Our studies of the interconversion between $Fe_2(\mu\text{-}O)_2$ and $Fe_2(\mu\text{-}O)(\mu\text{-}OH)$ core can thus serve as a basis for future studies correlating core protonation states and reactivity.

Acknowledgment. This work was supported by the National Institutes of Health (GM-38767). The National Science Foundation provided funds for the purchase of the Siemens SMART system. We thank Professor J. D. Britton for his generous help in the crystal structure determinations.

Supporting Information Available: Tables of crystallographic experimental details, atomic coordinates, thermal parameters, bond lengths, and bond angles; thermal ellipsoid figures (S1−S5) for all crystal structures we report in this paper, figures (S6 and S7) showing the temperature-dependent magnetic susceptibility of **1c**, **2c**, and **2f**, and a figure (S8) showing the resonance Raman study on the equilibrium between **2f** and **5f**. A CIF file of the crystallographic information is also available. This material is available free of charge via the Internet at http://pubs.acs.org.

JA983615T

(54) Holland, P. L.; Wilkinson, E. C.; Mahapatra, S.; Rodgers, K. R.; Que, L., Jr.; Tolman, W. B. Results to be published.
(55) Wing, R. M.; Callahan, K. P. *Inorg. Chem.* **1969**, *8*, 871−874.
(56) Ling, J.; Farooq, A.; Karlin, K. D.; Loehr, T. M.; Sanders-Loehr, J. *Inorg. Chem.* **1992**, *31*, 2552−2556.
(57) Sitter, A. J.; Shifflett, J. R.; Terner, J. *J. Biol. Chem.* **1988**, *263*, 13032−13038.
(58) Asher, S. A.; Vickery, L. E.; Schuster, T. M.; Sauer, K. *Biochemistry* **1977**, *16*, 5849−5854.
(59) Debois, A.; Lutz, M.; Banerjee, R. *Biochemistry* **1979**, *18*, 1510−1517.